Rational Design, Structure, and Biological Evaluation of Cyclic Peptides Mimicking the Vascular Endothelial Growth Factor

Victor Goncalves,[†,‡,§] Benoit Gautier,[†,‡,§] Pascale Coric,[||,⊥] Serge Bouaziz,[||,⊥] Christine Lenoir,[‡,§] Christiane Garbay,[‡,§] Michel Vidal,[*,‡,§] and Nicolas Inguimbert[*,‡,§]

Université Paris Descartes, UFR biomédicale, Laboratoire de Pharmacochimie Moléculaire et Cellulaire, 45 rue des Saints Pères, Paris, F-75006, France, INSERM U648, 45 rue des Saints Pères, Paris, F-75006, France, Université Paris Descartes, UFR de pharmacie, Laboratoire de Pharmacologie Chimique et Génétique, 4, avenue de l'Observatoire, Paris, F-75006, France, and INSERM U640, Paris, F-75006, France

Received June 15, 2007

Angiogenesis is the development of a novel vascular network from a pre-existing structure. Blocking angiogenesis is an attractive strategy to inhibit tumor growth and metastasis formation. Based on structural and mutagenesis data, we have developed novel cyclic peptides that mimic, simultaneously, two regions of the VEGF crucial for the interaction with the VEGF receptors. The peptides, displaying the best affinity for VEGF receptor 1 on a competition assay, inhibited endothelial cell transduction pathway, migration, and capillary-like tubes formation. The specificity of these peptides for VEGF receptors was demonstrated by microscopy using a fluorescent peptide derivative. The resolution of the structure of some cyclic peptides by NMR and molecular modeling has allowed the identification of various factors accounting for their inhibitory activity. Taken together, these results validate the selection of these two regions as targets to develop molecules able to disturb the development of cancer and angiogenesis-associated diseases.

Introduction

Angiogenesis is the new blood vessel formation from a pre-existing endothelial structure. During embryonic development, endothelial cells are particularly active, while during adult life they are usually limited to physiological processes such as wound healing and menstrual cycle. The deregulation of angiogenesis is involved in several pathologies including cancer, ischemic, and inflammatory diseases (atherosclerosis, rheumatoid arthritis, or age-related macular degeneration).[1,2] Consequently, the research for drugs able to disrupt abnormal angiogenesis constitutes an essential research field.[3,4]

Angiogenesis is tuned by pro-angiogenic and antiangiogenic factors, and the shift from this equilibrium leads to pathological angiogenesis. Among these factors, the vascular endothelial growth factor (VEGF,[a] also called VEGF-A) plays a major role in angiogenesis.[5] VEGF and its structural homologues, VEGF-B, -C, -D, -E, and -F and PlGF (placenta growth factor), are homodimeric glycoproteins that belong to the cystine knot protein class (Figure 1). There are at least eight known human isoforms of VEGF-A resulting from the alternative RNA splicing. The predominant isoform in humans is named $VEGF_{165}$, according to its length in amino acids. The pro-angiogenic function of $VEGF_{165}$ is mediated through binding to two tyrosine kinase receptors, VEGF receptor 1 (VEGF-R1, Flt-1) and VEGF receptor 2 (VEGF-R2, KDR).[6] These receptors are located at the surface of endothelial cells and various tumor cell types. $VEGF_{165}$ binds to VEGF-R1 (10−30 pM), with higher affinity compared to VEGF-R2 (100−700 pM).[7] Different biological roles have been suggested for these two receptors. VEGF-R2 is the major mediator of the mitogenic, angiogenic, and

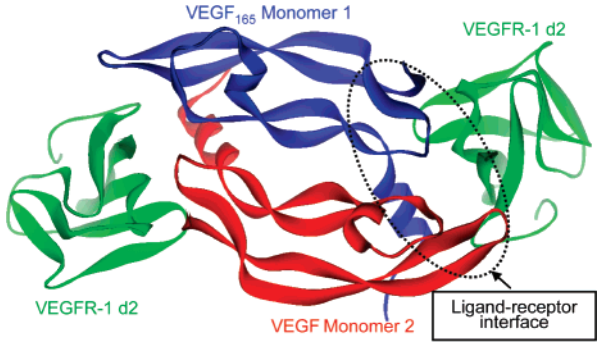

Figure 1. X-ray structure of $VEGF_{8-109}$ in complex with VEGF-R1 d2.

* To whom correspondence should be addressed. Dr. Nicolas Inguimbert and Pr. Michel Vidal, Laboratoire de Pharmacochimie Moléculaire et Cellulaire, Université Paris Descartes, 45 rue des Saints Pères, FR-75006 Paris, France. Tel.: +33.1.42.86.21.26 (N.I. and M.V.). Fax: +33.1.42.86.40.82 (N.I. and M.V.). E-mail: nicolas.inguimbert@univ-paris5.fr (N.I.); michel.vidal@univ-paris5.fr (M.V.).

† Victor Goncalves and Benoit Gautier participated equally to this work.

‡ Université Paris Descartes, UFR biomédicale.

§ INSERM U648.

|| Université Paris Descartes, UFR de pharmacie.

⊥ INSERM U640.

[a] Abbreviations: Acm, acetamidomethyl; AcOH, acetic acid; COSY, correlation spectroscopy; DCM, dichloromethane; DIPEA, *N*,*N*′-diisopropylethylamine; DMF, dimethylformamide; DMSO, dimethylsulfoxide; DQF-COSY, double quantum filtered-correlation spectroscopy; ECD, extracellular domain; EDT, ethanedithiol; EDTA, ethylenediaminetetraacetic acid; EGTA, ethylene glycol-bis(2-aminoethylether)-*N*,*N*,*N*′,*N*′-tetraacetic acid; Flt-1, fms-like tyrosine kinase-1; ERK, extracellular signal-regulated kinase; FBS, foetal bovine serum; Fmoc, fluorenylmethyloxycarbonyl; HBTU, O-benzotriazole-*N*,*N*,*N*′,*N*′-tetramethyl-uronium-hexafluoro-phosphate; Hca, L-(7-hydroxycoumar-4-yl)alanine; hF, homophenylalanine; HMP resin, 4-(hydroxymethyl)phenoxymethyl-copoly(styrene-1%divinylbenzene) resin; HNTG, hepes-NaCl-triton-glycerol; HOBt, *N*-hydroxybenzotriazole; HUVEC, human umbilical vein endothelial cell; Ig, immunoglobulin; KDR, kinase domain-containing receptor; MAPK, mitogen-activated protein kinase; NMP, 1-methyl-2-pyrrolidinone; NOE, nuclear Overhauser effect; NOESY, nuclear Overhauser enhancement spectroscopy; PBS, phosphate buffer saline; Rink amide MBHA, 4-(2′,4′-dimethoxyphenyl-Fmoc-aminomethyl)-phenoxyacetamido-methylbenzhydryl amine; rmsd, root mean square deviation; SDS, sodium dodecyl sulphate; SPPS, solid-phase peptide synthesis; TBS, tris-HCl buffer saline; TBST, tris-HCl buffer saline tween 20; TFA, trifluoroacetic acid; TIPS, triisopropylsilane; TOCSY, total correlated spectroscopy; VEGF, vascular endothelial growth factor; VEGF-R, vascular endothelial growth factor receptor; VEGF-R1 d2, vascular endothelial growth factor receptor 1 domain 2.

10.1021/jm0706970 CCC: $37.00
Published on Web 09/27/2007

permeability-enhancing effects of $VEGF_{165}$. In contrast, VEGF-R1 is a negative regulator of angiogenesis during early development, but plays an important role in angiogenesis under pathological conditions.[8,9] Recent studies have shown that both are necessary for human tumor growth and metastasis formation.[10,11] Another tyrosine kinase receptor, VEGF receptor 3, responsible for lymphangiogenesis, has been proved to be also involved in tumor angiogenesis and growth.[12] More recently, neuropilin-1 (NP-1), a nontyrosine kinase receptor of $VEGF_{165}$ has been identified on endothelial and tumor cells. NP-1 acts as a co-receptor, enhancing the activity of VEGF-R2.[13] Considering the central role displayed by the system $VEGF_{165}$-VEGF receptors in pathological angiogenesis, these proteins constitute attractive and well-established targets for the development of antiangiogenic therapies aiming to disrupt their interaction. One prominent example is the humanized recombinant monoclonal antibody called bevacizumab. It has been approved as a therapeutic antiangiogenic agent, in particular, for treatment of metastatic colorectal and non-small cell lung cancer.[14] Most of chemical approaches are constituted by the inhibition of the VEGF receptors tyrosine kinase activity and several compounds are currently under clinical evaluation.[15] Nevertheless, most of them are not specific and inhibit other tyrosine kinase receptors. Other methods inhibiting the VEGF activity are to produce soluble VEGF-R1 or VEGF-R2, acting as a VEGF trap,[16] VEGF receptor specific ribozyme,[17] and RNA aptamers against VEGF.[18] On the other hand, several peptides binding to the extracellular domain (ECD) of the receptor constituted by seven immunoglobulin (Ig)-like domains have been reported to modulate VEGF-dependent angiogenesis. A large number of them exhibit antagonist behavior and only few acts as agonists. Most of these antagonists were discovered either by phage display screening or combinatorial peptide libraries.[19,20]

Despite the numerous reports dealing with the characterization of the VEGF/VEGF receptors interface, the rational design of peptides modulating this interaction is relatively rare. A first approach, developed by Jia et al.,[21] consisted in testing the affinity for the VEGF receptors of 12-amino acid peptides corresponding to fragments of $VEGF_{189}$. Among identified antagonist peptides, the most effective one was based on the sequence 11−22 (HHEVVKFMDVYQ-NH_2) of $VEGF_{189}$ and exhibited an IC_{50} of 42 μM on a competition binding assay with VEGF-I^{125}. Other rational strategies for the discovery of VEGF receptor ligands are based on the knowledge of the structure of the interface between VEGF and VEGF-R1,2. These strategies were made possible thanks to the availability of deletion studies performed on the ECD of VEGF-R1,[22−27] of crystallographic structures of $VEGF_{165}$ alone[28] or in complex with VEGF-R1 domain 2[22] (VEGF-R1 d2), as well as the structure of PlGF[29] in interaction with VEGF-R1 d2. In addition, site-directed mutagenesis experiments allowed the identification of $VEGF_{165}$ binding determinants with VEGF-R1 and VEGF-R2.[28,30]

These studies showed that VEGF binds as an antiparallel homodimer to two copies of VEGF receptors and that the ECD 2 is mainly responsible for VEGF binding. The surface of interaction is represented by about 65% for the monomer 1 and 35% for the monomer 2 of the VEGF, respectively (Figure 1). The fragments of the monomer 2 directly in contact with the receptor are the β-sheet 46−48 and the loop 79−91. The sequence 79−93 was used as a model by Zilberberg et al. to design a 17-amino acid cyclic peptide, cyclo-VEGI (head-to-tail c[DFPQIMRIKPHQGQHIGE]-NH_2),[31,32] which proved to be an antagonist of VEGF receptors with an IC_{50} of 12 μM measured on BAE cells. On the other hand, the $VEGF_{165}$ monomer 1 (65% of the surface of contact) interacts mainly with the receptors through two fragments: the N-terminal α-helix 16−27 and the loop 61−68 (Figure 2). D'Andrea et al. proposed a peptide mimicking the α-helix 16−27 region,[33] and according to structural and mutagenesis data, they suggested that the affinity of this fragment relied essentially on the interaction of the residues F17, M18, Y21, Q22, and Y25 with the receptors. After forcing the domain to adopt a helical structure in solution, surprisingly, the peptide (Ac-KVKFMD-VYQRSYCHP-NH_2) revealed to act as an agonist of both VEGF-R1 and VEGF-R2.

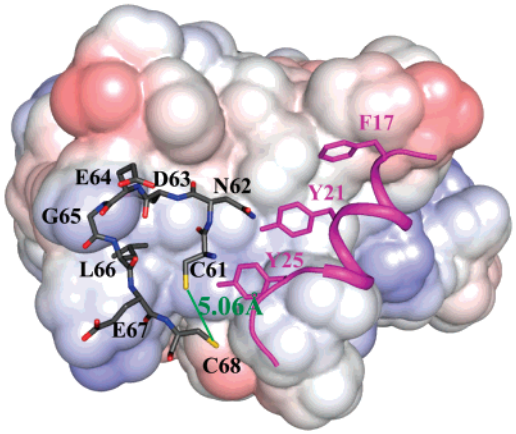

Figure 2. X-ray structure of VEGF fragments 16−27 (magenta) and 61−68 (gray) in complex with VEGF-R1 d2. The colored surface represents the electrostatic potential of VEGF-R1 d2 surface.

Up to now, the loop 61−68 (CNDEGLEC) has never been used to design inhibitors. Yet, the X-ray structure of $VEGF_{8-109}$ with VEGF-R1 d2 showed that the residue D63 participates in the unique direct charge-mediated interaction existing between the ligand and it receptors (with R224 of VEGF-R1). Moreover, the alanine-scan analysis of VEGF mutants highlighted that the region 63−67 of VEGF constitutes a hot-spot for VEGF-R1 binding, as confirmed by the 30-fold decrease of affinity observed for the mutations D63A/E64A/E67A.[30]

Herein, we report the rational design of the first cyclic peptides based on the structure of the region 61−68, their optimization and the NMR study of two active and inactive peptides accounting for their different activity. Furthermore, a fluorescent peptide was synthesized to verify the specificity of the interaction on endothelial cells. Finally, the antagonist activity of the most active peptides was verified on different cell assays.

Results and Discussion

Testing of the Peptide Fragments 61−68 and 16−27 as Potential VEGF Receptor Antagonists. In the first instance, we searched to define if the VEGF sequences 61−68 and 16−27 could constitute templates for the design of VEGF receptors antagonists. In this purpose, we synthesized, first, the linear peptide **1** (SNDEGLES), based on the sequence of the region 61−68, by standard N^{α}-Fmoc chemistry on HMP resin.[34] To avoid oxidation issues, the cysteines 61 and 68 were replaced by two serines. Couplings were carried out with in situ-activating reagents (HBTU, HOBt in the presence of DIPEA) to generate HOBt esters (Table 1).

Furthermore, in the VEGF, the region C61−C68 adopts a pseudocyclic structure, with only 5 Å separating the thiol functions of the N- and C-terminal cysteines (Figure 2). Therefore, we searched to mimic the active conformation by synthesizing a cyclic peptide constrained by a disulfide bridge.

Table 1. Sequence and Inhibitory Potency of the Peptides **1**−**3** and **SP5.2** on VEGF-R1

entry	sequence	activity at 400 μM[a]
1	SNDEGLES	24.3 ± 3.9
2	Ac-c[CNDEGLEC]-NH_2	39.8 ± 1.3
3	KFMDVYQRSYCH-NH_2	47.3 ± 6.5
SP5.2	NGYEIEWYSWVTHGMY-NH_2	99.2 ± 0.4

[a] Activity corresponds to the percentage of biotinylated $VEGF_{165}$ displaced by the indicated concentration of peptide on VEGFR-1. In this assay, $VEGF_{165}$ displayed an IC_{50} of 387 ± 60 pM.

Scheme 1. Synthesis of the Peptide **2**

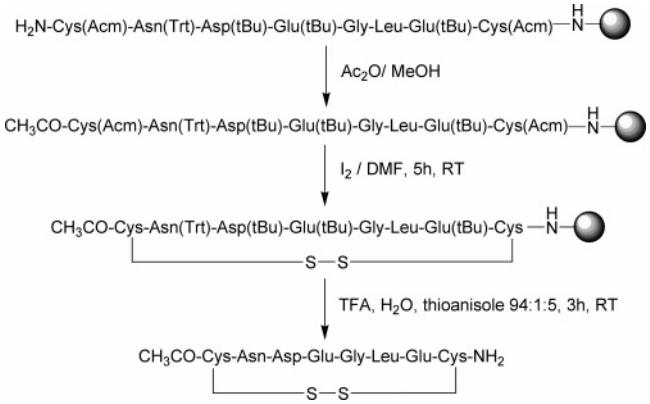

Cysteines were introduced as *S*-acetamidomethyl (Acm)-protected amino acids, because treatment of such residues by iodine results in simultaneous removal of the sulfhydryl protecting groups and disulfide bond formation (Scheme 1). Preliminary experiments demonstrated that iodine oxidation of the peptide containing a cysteine residue with a free N^{α}-amino function was sluggish, thus we chose to perform a *N*-acylation of C61 with acetic anhydride before oxidizing the peptide. Moreover, a systemic issue in oxidizing cysteine-containing peptides is the formation of dimer and polymer products due to cross-reaction between peptide chains. To limit this problem, the cyclization was performed on resin (substitution: 0.6 mmol/g) with an excess of iodine in DMF.[35] In this way, each peptide chain supported by the resin was relatively separated from the others, favoring intrachain resin-bound reaction by taking advantage of the pseudodilution phenomenon.[36] Final peptide **2** (Ac-c[CNDEGLEC]-NH_2) was obtained after cleavage and deprotection of the resin, with thioanisole and triisopropylsilane (TIPS) as scavengers.

As references for screening assays, we also synthesized the peptide **3** (KFMDVYQRSYCH-NH_2), which corresponds to the sequence of the α-helix 16−27, and the peptide **SP5.2**[37] identified by phage-display library screening and described in the literature as a VEGF-R1 antagonist.

Peptides affinity for VEGF-R1 was evaluated by a chemiluminescent assay relying on competition between the tested compound and biotinylated $VEGF_{165}$ for binding to recombinant receptor 1[38] (Table 1). The linear peptide **1** appeared as a weak ligand of VEGF-R1 with 24% inhibition of $VEGF_{165}$ binding at 400 μM. As expected, the cyclization of this peptide led to a small increase of its binding properties with 40% inhibition observed at the same concentration for the peptide **2**. The peptide **3**, mimicking the α-helix, was slightly more potent (47% of inhibition at 400 μM), while **SP5.2** was clearly active with an IC_{50} of 28 μM. Unlabeled $VEGF_{165}$ was used as internal control and exhibited in this assay an IC_{50} of 387 ± 60 pM. Taken together, the results obtained for the peptide **2** and **3** confirm the accuracy of choosing the sequence 61−68 as a template for developing antagonists of the VEGF−VEGF receptors interaction.

Scheme 2. Synthesis of the Peptide **7**

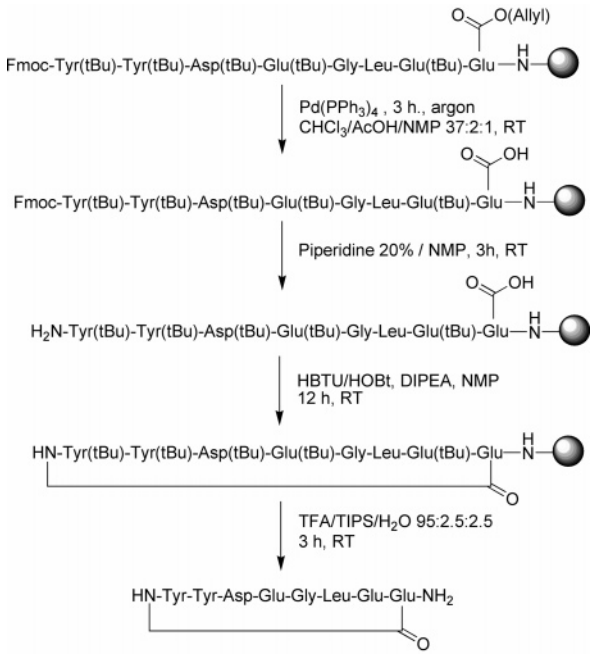

Optimization of the Peptide 2 by Rational Design of New Cyclic Peptides. Considering the weak affinity of the peptide **2** for the receptor 1, we searched to improve its activity by targeting simultaneously the domains of interaction 61−68 and 16−27. Indeed, mutagenesis data show[28] that alanine-substitution of the three aromatic residues F17, Y21, and Y25 of VEGF leads to a decrease of the affinity of the mutant compared to the wild type protein. As the loop 61−68 is in close proximity with the aromatic residues Y21 and Y25, we hypothesized that the amino acids C61 and N62, not essential for the interaction, could be advantageously replaced by two aromatic amino acids. Therefore, the cyclic scaffold of the 61−68 region was conserved as well as the determinant residues for interaction (D63, E64, and E67) and two new aromatic residues were introduced to mimic the position of the tyrosines in the α-helix (Figure 2). Given the fact that the cysteines needed to be suppressed, we replaced the previous disulfide bridge by a lactam cyclization between the free amino-function of the N-terminal aromatic residue and the side-chain carboxylic acid function of a glutamic acid introduced in place of C68. In addition to limit the backbone flexibility, this modification tends to increase the biological stability of the cyclic peptides. Based on this general scaffold, we synthesized a series of peptides differing by the nature of the amino acids used in position 61, 62, and 66, and the length of the cyclic backbone.

As previously, we chose to perform cyclization with the peptides anchored on resin to prevent formation of byproducts. The synthesis was carried out on Rink amide MBHA resin using Fmoc chemistry (Scheme 2). Amino acids were introduced with acid-labile protecting groups, except for the C-terminal glutamic acid whose side chain was protected by an allyl group. Once the elongation was completed, the allyl protecting group was removed by Pd(0)-catalyzed allyl transfer[39] using $Pd(PPh_3)_4$ in $CHCl_3$/AcOH/NMP (37:2:1) under argon atmosphere. The N^{α}-Fmoc group was then eliminated by piperidine treatment in NMP, and the lactam cyclization was performed overnight using traditional reagents, HBTU/HOBt/DIPEA in NMP/DCM. The

Table 2. Sequence and Inhibitory Potency of the Peptides **4**−**12** on VEGF-R1

entry	sequence[a]	activity at 100 μM[b]	IC_{50}[c] (μM)
4	c[homoPhe-homoPhe-Asp-Glu-Gly-Leu-Glu-Glu]-NH_2	0.0 ± 2.6	N/D
5	c[homoPhe-homoPhe-Asp-Glu-Gly-Leu-Glu]-NH_2	34.9 ± 0.1	N/D
6	c[Phe-Phe-Asp-Glu-Gly-Leu-Glu-Glu]-NH_2	37.9 ± 6.6	N/D
7	c[Tyr-Tyr-Asp-Glu-Gly-Leu-Glu-Glu]-NH_2	57.1 ± 2.3	39.9 ± 16.6
8	c[Tyr-Trp-Asp-Glu-Gly-Leu-Glu-Glu]-NH_2	4.8 ± 4.3	N/D
9	c[Glu-Tyr-Asp-Glu-Gly-Leu-Glu-Glu]-NH_2	0.6 ± 7.0	N/D
10	c[Tyr-Tyr-Asp-Glu-Gly-Tyr-Glu-Glu]-NH_2	16.6 ± 5.2	N/D
11	c[Tyr-Hca-Asp-Glu-Gly-Leu-Glu-Glu]-NH_2	1.7 ± 3.9	N/D
12	c[homoPhe-Hca-Glu-Gly-Leu-Glu-Glu]-NH_2	87.3 ± 1.4	19.3 ± 6.8

[a] homoPhe, homophenylalanine; Hca, L-(7-hydroxycoumar-4-yl)alanine. [b] Activity corresponds to the percentage of biotinylated $VEGF_{165}$ displaced by the indicated concentration of peptide on VEGF-R1. [c] N/D = not determined.

remaining side chain protecting groups were then removed, and the peptide was cleaved from the resin under acidic conditions.

We first synthesized the peptide **4**, which possesses two homophenylalanines as aromatic amino acids. Indeed, based on docking studies, it appeared necessary to introduce a relatively long side chain on these positions to mimic the distant location of the original Y21 and Y25. Unfortunately, once tested on our competition assay, the peptide **4** revealed to be inactive on VEGF-R1 at 100 μM (Table 2). We searched if we could improve the affinity for the receptor by restricting the flexibility of the cyclic backbone. With this aim, we constructed the peptide **5** where E67 was suppressed. This peptide appeared as a weak ligand of VEGF-R1 with 35% inhibition of $VEGF_{165}$ binding at 100 μM. Based on these results, we proposed that the inactivity of the peptide **4** may not be necessarily related to the excessive length of the backbone but rather to the too distant position of the aromatic rings carried by the homophenylalanines. Thus, we synthesized the peptide **6**, which bears two phenylalanines in place of the homophenylalanines and whose E67 was conserved in the backbone. This peptide proved to be as active as the peptide **5**.

Therefore, we chose to conserve this eight-amino acid backbone and to study the effect of the nature of the aromatic amino acids on the affinity of the cyclic peptides. We synthesized the peptides **7** and **8** whose aromatic residues were, respectively, YY and YW. The inherent idea was that the peptide **7** could mimic the Y21 and Y25 amino acids present in $VEGF_{165}$, while the peptide **8** contains the two amino acids W21 and Y25 found in the PlGF. The peptide **7** appeared to be the most active one on VEGF-R1 displacement assay, with an IC_{50} of 40 μM, whereas the peptide **8** was unable to compete with biotinylated $VEGF_{165}$ binding even at 100 μM. We followed the structure−activity relationship study by testing the affinity of the peptide **9** with the same sequence as that for peptide **7**, except the first tyrosine residue, which was replaced by a glutamic acid because in the VEGF the Y25 is close to the side chain amino function of K171 from VEGF-R1 d2. This modification was supposed to introduce a supplementary electrostatic interaction between the carboxylate function of the glutamic acid and the K171 amino function, but unfortunately, the peptide **9** showed to be inactive on VEGF-R1. A final assay resulted in producing the peptide **10** bearing two tyrosines as aromatic residues and where L66 was replaced by another tyrosine with the aim to establish a new π-stacking interaction with the nearby Y199 within the receptor. Although conserving a weak affinity to VEGF-R1, the peptide **10** was less active than the previous peptide **4**.

To sum up this structure−activity relationship study, the results obtained above confirmed our rational approach because the introduction of aromatic amino acids in the initial cyclic scaffold led to a strong improvement of the peptide affinity, compared to the isolated fragments **2** and **3**. However, cyclic peptides affinity seems to be strongly dependent on the nature of the aromatic amino acids present on their sequence, because modifications of steric hindrance can induce loss of the activity (see the peptide **7** compared to the peptide **8**). A comparison of the peptides **7** (tyrosine−tyrosine) and **10** (glutamic acid−tyrosine) tends to prove that the affinity is dependent on the presence of two aromatic residues at these positions, probably to establish the hydrophobic interactions originally existing between Y21 and Y25 and the residues L221, L204, and F172 of the receptors. Moreover, the presence of an H-bond donor/acceptor function on the cycle of the second aromatic residue seems important for interacting with the amino function of K171.

Table 3. NMR Chemical Shifts of the Peptides **4** and **7**[a]

residues	chemical shifts (ppm) NH	αH	βH	others
(A) Peptide **4** in 10% DMSO-d_6, 10% D_2O, and 80% H_2O at 293 K, pH 4.1				
hF1	8.08	4.25	1.94	γCH_2 2.13, 2.71; ϵH 7.27; ηH 7.26; ζH 7.35
hF2	8.45	4.03	2.08	γCH_2 2.63, 2.72; ϵH 7.24; ηH 7.22; ζH 7.32
D3	8.57	4.47	2.82, 2.89	
E4	8.15	4.27	1.94	γCH_2 2.16, 2.34
G5	8.12	3.73, 3.95		
L6	7.90	4.33	1.63	γCH 1.56; δCH_3 0.84
E7	8.30	4.22	1.97	γCH_2 2.11, 2.41
E8	8.22	4.22	β_1 1.94	$\gamma_1 CH_2$ 2.13, 2.4; $\gamma_2 CH_2$ 7.18, 7.48
(B) Peptide **7** in 10% DMSO-d_6, 10% D_2O, and 80% H_2O at 293 K, pH 4.24				
Y1	8.05	4.45	2.72, 2.9	δH 7.00; ϵH 6.77
Y2	8.25	4.3	2.94, 3.03	δH 7.05; ϵH 6.80
D3	8.35	4.45	2.67, 2.78	
E4	8.14	4.26	1.95, 2.16	γCH_2 2.37
G5	8.18	3.82, 3.94		
L6	7.96	4.32	1.65	γCH 1.58; δCH_3 0.84
E7	8.39	4.21	1.99, 2.11	γCH_2 2.41
E8	8.09	4.11	$\beta_1$1.82, 1.94	$\gamma_1 CH_2$ 2.26; $\gamma_2 CH_2$ 7.11,7.39

[a] Peptides **4** and **7** were prepared in 10% D_2O/H_2O and 10% DMSO at pH 4.1 and 4.24, respectively. These values were referenced to the water signal at 4.8 ppm and were determined from 2D ^{1}H TOCSY spectra recorded at 293 K and 600 MHz.

To identify the factors favoring the binding of the cyclopeptides on the VEGF-R1 and how this binding could perturb the interaction between the VEGF and its receptor VEGF-R1, the peptides **4** and **7** have been studied by NMR and the peptide **7**, which was shown to have the highest affinity, was docked on VEGF-R1 to compare the formation of the complexes.

1D and 2D Proton NMR Experiments on the Cyclic Peptides 4 and 7. The 1D proton NMR spectra performed on the two cyclic peptides **4** and **7** show very well-resolved spectra with no overlaps, making the assignment easy to complete

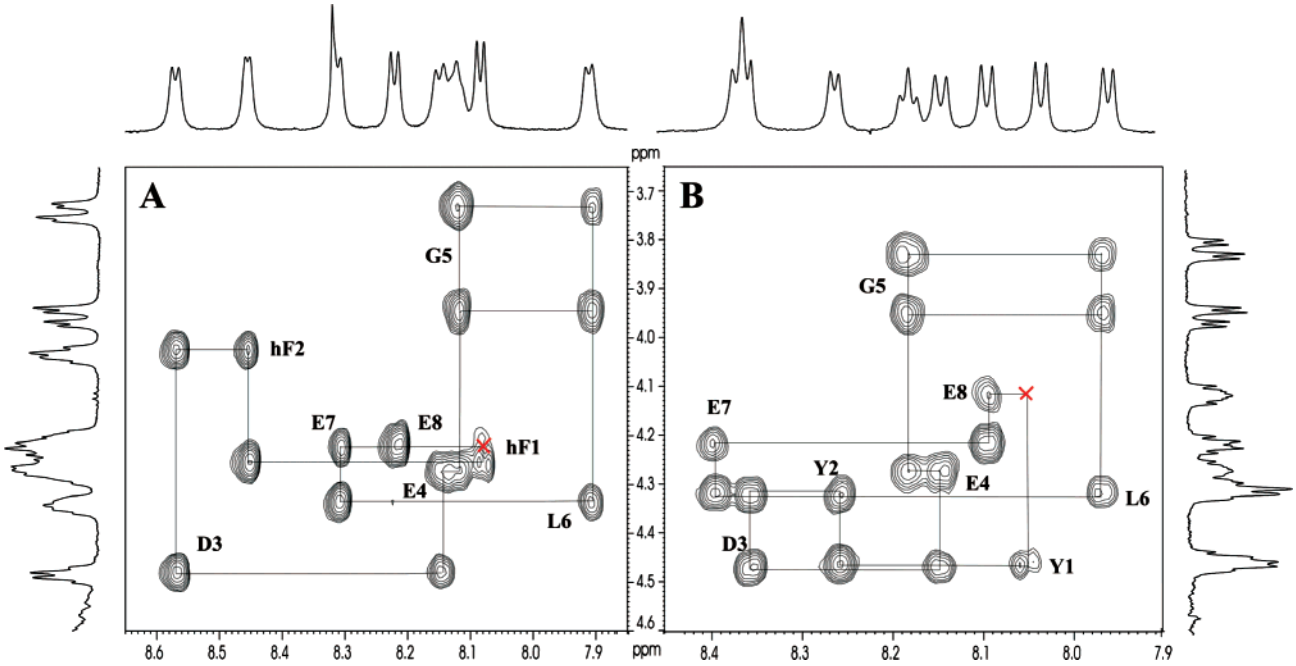

Figure 3. ^{1}H NMR spectra representing the correlations between Hα protons (vertical 1D spectra) and amide protons (horizontal 1D spectra) in a NOESY experiment (2D spectra), with a 250 ms mixing time. Spectra were recorded in a solvent mixture H_2O/D_2O/DMSO-d_6 (80:10:10), at pH 4.1 and 4.24, respectively, for the two cyclic peptides **4** (A) and **7** (B), at a temperature of 293 K. Intraresidual and sequential correlations between NH(i + 1) and Hα(i) protons can be followed from residue Y1 or hF1 to E8. Red crosses show the correlation between the first (Y1 or hF1) and the last (E8) residues in the cyclic peptide.

(Table 3). In particular, the amide regions (Figure 3A,B) are well-resolved for both peptides **4** (7.90 to 8.57 ppm) and **7** (7.96 to 8.39 ppm). The aromatic region is less well-resolved for the peptide **4** (7.22 to 7.35 ppm) compared to peptide **7** (6.77 to 7.05 ppm; Table 3). The 2D proton NMR spectra allowed us to identify the different spin systems thanks to the TOCSY and DQF-COSY experiments. Those spin systems have been sequentially correlated through the nuclear Overhauser enhancement spectroscopy (NOESY) experiment that gives the correlation between amino acids through space (Figure 3A,B). For each peptide, the NOESY experiment has confirmed that the peptide is cyclic by observing a distance proximity between the hF1-(HN) and the E8(Hα) in the peptide **4** (red cross in Figure 3A) and between the Y1(HN) and the E8(Hα) at a less extent in the peptide **7** (red cross Figure 3B). This particular correlation can be evidenced only by increasing the scale of the spectra (Figure 3B). It is important to note that the chemical shift spreading is more significant for the peptide **4** compared to the peptide **7** in the amide region as well as for the Hα region (Figure 3A,B). Because the majority of the amino acids are identical within the two molecules except residues 1 and 2, we conclude that the two tyrosines replacing the two homophenylalanines produce an effect on the global conformation of peptide **7**.

NMR Analysis and NOE Restraints. DQF-COSY and TOCSY experiments were used to identify the spin systems, and NOESY experiments were used for sequential and long-range distance assignment.[40] No major overlaps occur in the amide or aliphatic regions, and characteristic intraresidual and sequential connectivities have been identified for all residues of the peptides **4** and **7** (Figure 3). The analysis of the NOEs allows to state that the two molecules adopt a different conformation because the number of NOEs identified on the peptide **4** (100) is more important than the one observed for peptide **7** (89). Of these distances, 62 are intraresidual, 31 are sequential, and 7 are medium range ($|i - j| \leq 4$) for the peptide **4**, while 63, 25, and 1 were found for peptide **7**. While the number of intraresidual constraints is equivalent for both peptides, the number of medium range constraints ($|i - j| \leq 4$) is higher for the peptide **4** than for peptide **7**. These medium range constraints are undoubtedly at the origin of the different folds adopted by the two peptides **4** and **7**. It is unexpected that

Table 4. Structural Statistics for the Peptides **4** and **7**

	peptide **4**	peptide **7**
(a) Restraints for Calculation		
total NOE restraints	100	89
intraresidue	62	63
sequential ($\|i - j\| = 1$)	31	25
medium range ($\|i - j\| \leq 4$)	7	1
(b) Structure Statistics		
rmsd		
bonds (Å)	(2.04−3.34) × 10^{-3}	(1.94−2.45) × 10^{-3}
bond angles (°)	0.51−0.6	0.49−0.53
improper torsions (°)	0.3−0.34	0.26−0.28
NOE restraints (Å)	(3.09−4.9) × 10^{-2}	(3.7−4.94) × 10^{-2}
(c) Final Energies (kcal/mol)		
E total	21.2−26.39	19.84−22.3
E bonds	0.56−1.49	0.49−0.77
E angles	9.45−13.22	8.22−9.8
E improper angles	1.03−1.385	0.75−0.87
E van der Waals	2.3−3.3	1.33−2.99
E NOE	4.79−12.02	6.12−10.87
(d) Ramachandran Plot		
residues in most favorable regions (%)	20	38
residues in additional allowed regions (%)	56	42
residues in generously allowed regions (%)	24	16
residues in disallowed regions (%)	0	4
(e) Atomic rmsd (Å) on the Backbone Atoms		
pairwise	0.26 ± 0.15	0.58 ± 0.44
to mean structure	0.25 ± 0.12	0.47 ± 0.37

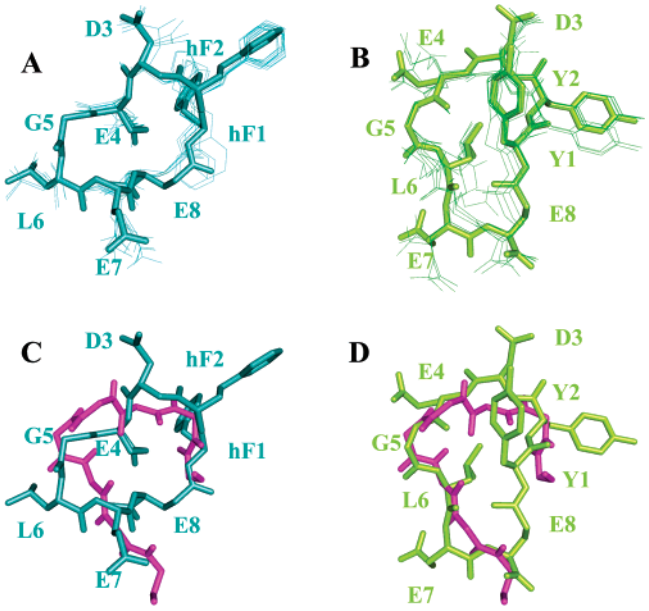

Figure 4. Comparison of the 3D structures of the cyclic peptides **4** and **7**. (A and B) Superimposition on the backbone atoms of the 10 best structures of the cyclic peptides **4** (cyan) and **7** (green), in line representation with the averaged structure in the stick representation. (C and D) Superimposition, on the backbone atoms, of the averaged structures of the cyclic peptide **4** (cyan) and **7** (green) with the structure of the fragment VEGF(61−68) (magenta) in the stick representation.

the replacement of two homophenylalanines by two tyrosines implicates such a modification on the backbone atoms and on side chain orientation. These data make us to conclude that the presence of one tyrosine or both of them is necessary to obtain an adequate conformation, providing an efficient inhibitory activity for peptide **7**. Moreover, the different number of restraints will have a consequence on the convergence of the structures (Table 4).

Structural Analysis of the Cyclic Peptides 4 and 7. The 3D structure calculations were performed using X-PLOR.[41,42] Out of 200 calculated structures, for each peptide, 10 were selected according to their low overall energy and their weak number of distance restraint violations. None of the structures exhibited an NOE violation greater than 0.2 Å and all of them revealed a good covalent geometry, with no bond or angle violations. The Ramachandran plots show that 100% of the residues are found in the allowed regions for the peptide **4**, while 4% of the residues (over 10 structures) were located in a disallowed region (Table 4d). The superimposition of the 10 lowest energy structures on their backbone atoms shows a good convergence of the structures for both peptides **4** and **7** (Figure 4A,B). The pairwise rmsd has been calculated for each family of structures and evaluated, respectively, to 0.26 ± 0.15 Å and 0.58 ± 0.44 Å on the backbone atoms from residues 1 to 8. The same measure performed relatively to the averaged structure, on the whole backbone atoms, gave a rmsd of 0.25 ± 0.12 Å and 0.47 ± 0.37 Å for the peptides **4** and **7**, respectively (Figure 4A,B). Input data for structural calculations and statistics are listed in Table 4.

According to the structural statistics, the final energies, and the Ramachandran plot results (Table 4), the two structures possess a good quality with a better convergence of the structures in the case of peptide **4** compared to peptide **7** (Figure 4A,B). These results could be due to a higher flexibility of peptide **7** and could explain why peptide **7** would be more active, by having a higher capacity to adapt to the VEGF-R1 target, compared to peptide **4**. The substitution of the two homophenylalanines by the tyrosines could account for the higher capacity of peptide **7** to adapt on the target VEGF-R1.

The amino acid side chains seem to point outside of the cyclic peptides except for residues E4 in peptide **4** and L6 in peptide **7**, which orients to the inside of the cycle. hF2 and Y2 are directed to the outside of the molecule while the hF1 and Y1 are folded under and above the plan of the cycle of peptide **4** and peptide **7**, respectively (Figure 4A,B). The folding of the hF1 under the plan of the cycle could prevent the interaction of peptide **4** with the receptor VEGF-R1, while the folding of Y1 above the cycle does not prohibit the interaction with the receptor VEGF-R1 but rather could stabilize this interaction.

The rmsd between the averaged structure of peptide **4** and the VEGF fragments 61−68 or 63−67 gives, respectively, a value of 2.68 Å and 2.43 Å on backbone atoms. The same calculations between peptide **7** and VEGF fragments 61−68 and 63−67 were evaluated to 1.69 Å and 1.59 Å, respectively (Figure 4C,D). These results show a better convergence between peptide **7** and the fragment VEGF compared to peptide **4**. These data could account for the higher affinity for the VEGF-R1 observed for peptide **7** compared to peptide **4**.

Analysis of the Intramolecular Hydrogen Bonds within VEGF and the Peptides 4 and 7. To bring an explanation

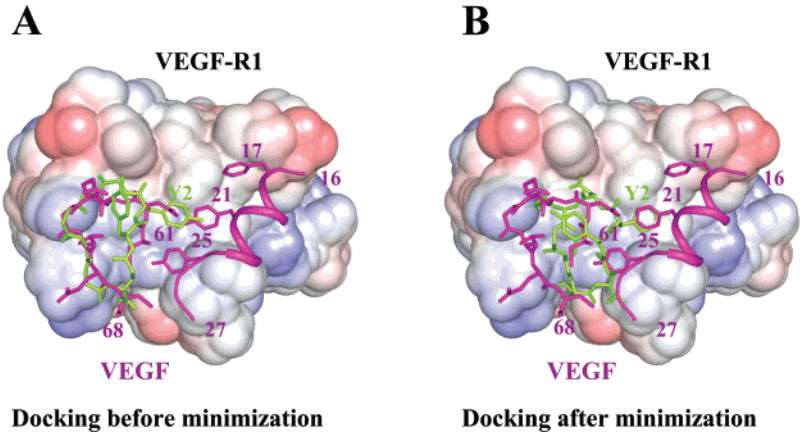

Figure 5. Superimposition of the average cyclic peptide **7** (green) with the VEGF fragment 61−68 (magenta) in the complex with VEGF-R1, which the surface is colored according the electrostatic properties of the amino acids. (A) The complex between VEGF-R1 and peptide **7** has not been energy minimized. (B) VEGF(61−68) and VEGF(16−27) were removed and the complex formed between the cyclic peptide **7** and VEGF-R1 was minimized without introducing NMR distance restraints. A slipping of the peptide **7** over VEGF-R1 is observed, allowing Y2 of peptide **7** to replace Y21 of VEGF 16−27.

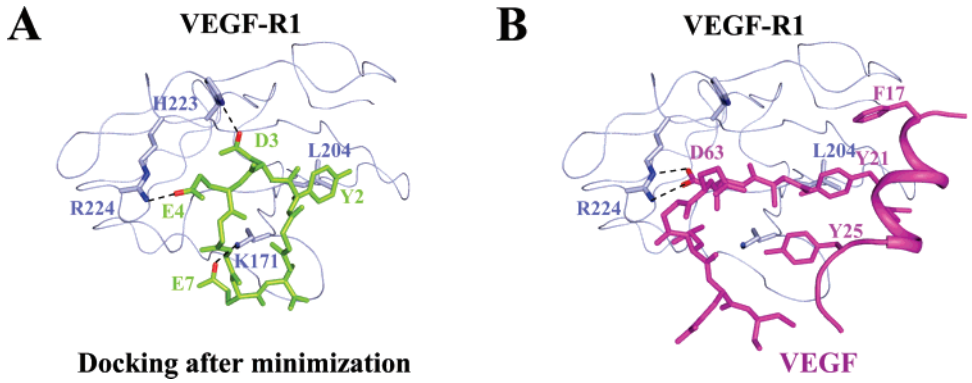

Figure 6. Comparison of the hydrogen bond network (in dotted lines) within the complexes formed between (A) VEGF-R1 and peptide **7** and (B) VEGF-R1 and VEGF(61−68). The receptor VEGF-R1 is represented as a blue trace and amino acid sidechains involved in hydrogen bonds (K171, H223, and R224) are in stick representation. The peptide **7**, in stick representation is colored in green and shows the amino acids implicated in hydrogen bonds (D3, E4, and E7). The domains of VEGF, (16−27) and (61−68), are colored in magenta.

concerning the different affinity and activity observed for peptide **7** and peptide **4** regarding VEGF-R1, the hydrogen bond network has been investigated for each peptide. Peptide **4** does not have any intramolecular hydrogen bond, while peptide **7** displays four intramolecular hydrogen bonds established as follows: Y1(ηH)/E4(Oϵ1), Y2(HN)/E8(Oϵ1), G5(HN)/E4(Oϵ1), and E7(HN)/E7-(Oϵ1). Only two intramolecular hydrogen bonds were found within VEGF fragment 61−68: L66(HN)/D63(O) and G65-(HN)/D63(Oδ1). It appears that, resulting from the formation of the cyclic peptide, the hydrogen bonds have been modified in peptide **7**. In spite of that, peptide **7** and VEGF 61−68 show a similar backbone conformation, in particular, if the corresponding fragments VEGF 63−67 and peptide **7**(3−7) are compared.

Docking of Peptide 7 on the VEGF-R1 Receptor. Finally, to compare the relative affinities of peptide **7** and VEGF concerning VEGF-R1 and to identify the factors necessary for the interaction, peptide **7** has been docked on the VEGF-R1 receptor and the complex has been submitted to energy minimization using the X-PLOR program. During the minimization, the VEGF-R1 d2 atom position was maintained fixed with the "constraints-fix" statement in X-PLOR, while the atoms of peptide **7** were free to move, and the constraints within peptide **7**, identified by NMR, have not been used. The results show that peptide **7**, docked on the VEGF-R1, slips on the surface of the VEGF-R1 receptor after minimization (Figure 5A,B), forms three hydrogen bonds with VEGF-R1, K171(Hζ1)/E7(Oϵ1), H223(Hδ1)/D3(Oδ1), and R224(ηH21)/E4(Oϵ2), and stabilizes this interaction (Figure 6A). The same analysis performed on the complex formed between the corresponding VEGF fragment 61−68 and VEGF-R1 shows that only two hydrogen bonds exist: R224(ηH22)/D63(Oδ1) and R224(Nϵ)/D63(Hδ2) (Figure 6B). The distribution of the hydrogen bonds, within the complex VEGF-R1/peptide **7**, could explain its affinity for the VEGF-R1 and the inhibitory properties of this cyclic peptide. All together, these data explain why the cyclic peptide **7** has such an efficient inhibitory activity compared to peptide **4** and, thus, how it could disturb the interaction between VEGF-R1 and VEGF by adapting on the receptor as a result of the formation of these hydrogen bonds. Moreover, Y2 in peptide **7** seems to disturb the interaction of the α-helix 16−27 with VEGF-R1, by taking the place of Y21 of VEGF (Figure 5 B). Finally, the interaction between peptide **7** and VEGF-R1 is mediated by hydrophobic contacts between Y2 of peptide **7** with L204 of VEGF-R1. This hydrophobic interaction was already observed in the complex VEGF/VEGF-R1 (Figure 6A,B).

The difference between peptide **4** and peptide **7** concerning their capacity to inhibit the interaction between VEGF and its receptor VEGF-R1 is clearly related to their conformation and their ability to adapt on the target VEGF-R1. First, the peptide **4** family has a better convergence than peptide **7**, with lower pairwise rmsd calculated on the whole backbone atoms, assuming that peptide **4** is less flexible than peptide **7**. Moreover, the larger number of medium range NOEs found for peptide **4** could contribute to the rigidity of peptide **4** comparatively to peptide **7**. These results show that the flexibility of the peptide is certainly necessary for an interaction with the VEGF-R1 receptor.

Second, the conformation of peptide **7** is closer to VEGF fragment 61−68 than peptide **4**, with a rmsd of 1.69 Å and 2.68 Å, respectively, calculated on the whole backbone atoms. This result confirms that the interaction with VEGF-R1 needs a flexibility of the peptide to adapt its target and inhibit the interaction with its original ligand.

Third, the presence of the tyrosines instead of the homophenylalanines seems to be of first consequence for the inhibitory activity of the peptide **7**. While the presence of the homophenylalanines in peptide **4** does not provide the inhibition of the interaction between VEGF and VEGF-R1, their replacement by tyrosines in peptide **7** supplies the inhibition. Peptide **7** disturbs not only the interaction of the domain VEGF 61−68 with VEGF-R1, but also the interaction of the α-helix 16−27 with VEGF-R1 because Y2 of peptide **7** prevents the contact of Y21 within VEGF(16−27) with the receptor VEGF-R1 by taking its place. This interaction seems to be directed by the hydrophobic properties of the aromatic cycle of Y21 able to interact with L204 of VEGF-R1 and be reinforced by the ability of Y2-(OH) to form a hydrogen bond.

Finally, another tyrosine, Y25, inside the VEGF segment 16−27, seems to be important for the interaction with the VEGF-R1 receptor. The optimization of the inhibitory properties of peptide **7** could go through a modification of its backbone to force the Y1 to locate on VEGF-R1 instead of Y25 of VEGF-(16−27) and to destabilize further the interaction between VEGF-R1 and VEGF, increasing the inhibitory activity of peptide **7**.

Microscopy Imaging of a Fluorescent Cyclic Peptide. After having demonstrated the binding properties of the cyclic peptides to VEGF-R1, we attempted to verify on a cellular model whether these peptides were specific to the VEGF receptors and, in this purpose, we developed a fluorescent-tagged peptide. However, because of the relative sensibility of our peptides to modifications of their sequence, it appeared that the use of common

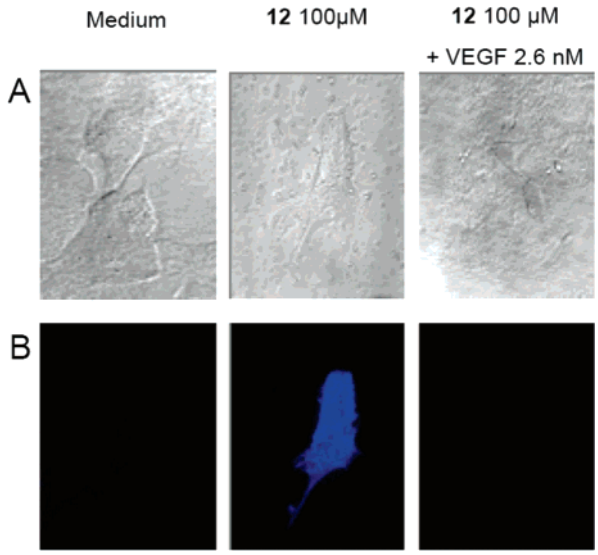

Figure 7. Imaging microscopy of VEGF receptor-specific binding of peptide **12** on HUVEC. Cells were incubated with or without 100 μM of peptide **12** in the presence or absence of an excess of VEGF (2.60 nM) over a period of 30 min. (A) Pictures taken by contrast phase with a biphotonic confocal microscope. (B) Fluorescence pictures by excitation at 700 nm with a biphotonic confocal microscope.

voluminous fluorescent dyes, such as the fluorescein introduced by El-Mousawi et al. for **SP5.2** labeling,[37] might lead to a loss of activity. Thereby, we chose to insert in the peptide, a L-(7-hydroxycoumar-4-yl)alanine (Hca), which is a fluorescent amino acid derivative developed by Brun et al.[43] This fluorophore is particularly well suited as it constitutes a good isostere of tyrosine or tryptophan. In addition, it is available as an N^{α}-Fmoc-protected amino acid allowing its introduction in the sequence by classical SPPS. First, we synthesized the compound **11** based on the sequence of peptide **7**, where an Hca was incorporated in place of the second tyrosine. This peptide did not displace VEGF binding even at 100 μM. By contrast, the peptide **12** (aromatic residues: hF-Hca) showed to be the most active peptide of the series, exhibiting an IC_{50} of 19.3 $\pm$ 6.8 μM. Thus, we used the peptide **12** to perform biphotonic microscopy experiments on human umbilical vein endothelial cells (HUVEC). First, we verified that no autofluorescence occurred in the absence of the peptide **12**. Then, after treatment by 100 μM of peptide **12** over a period of 30 min, a strong blue fluorescence was observed around the cells, demonstrating the binding properties of **12** on HUVEC. The incubation of HUVEC with the peptide **12** and an excess of VEGF during the same time period induced disappearance of the fluorescence. These results highlight the VEGF receptor-specific binding of **12** on HUVEC (Figure 7) and, by extension, the VEGF receptor-specificity of the series of cyclic peptides. Moreover, it allows us to consider this peptide as a valuable pharmacological tool for studies on the cellular becoming VEGF receptors or internalization of VEGF receptors.

Peptides Inhibit $VEGF_{165}$-Induced VEGF Receptors Signaling. After having confirmed on HUVEC the specific binding of the peptide **12** on VEGF receptors, we investigated whether the peptides **7** and **12**, which exhibited the best IC_{50} values on the binding assay, displayed antagonist activity on HUVE cells. Because the activation of ERK 1/2 pathway is required for the proliferative and migratory effects of VEGF on endothelial cells,[44] we examined the effects of these two peptides on $VEGF_{165}$-induced activation of ERKs 1/2 pathway. Each peptide tested at 100 μM caused a significant inhibition of $VEGF_{165}$-induced activation of ERKs 1/2 (Figure 8). **SP5.2**, chosen as

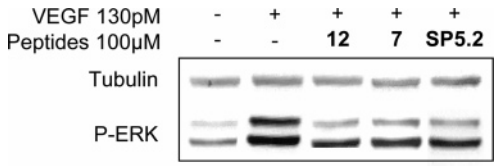

Figure 8. Inhibition of VEGF-induced p44/p42 ERK phosphorylation. Starved HUVEC, at confluence, were incubated with peptides **7**, **12**, and **SP5.2** at 100 μM over a period of 20 min and then stimulated by VEGF at 130 pM for 10 min. Western blot analysis was performed with antiphospho-p44/p42 ERK and anti-γ-tubulin. The figure shown is representative of three independent experiments.

reference for our activity tests, presented the same inhibition profile at 100 μM as that of the peptides **7** and **12**. This result validates the antagonist properties of peptides **7** and **12** and their ability to disrupt the signal transduction induced by VEGF.

Peptides Inhibit $VEGF_{165}$-Induced Cell Migration. Because designed peptides were able to block VEGF-induced ERK phosphorylation, we used the wound healing assay[31] to confirm the potential antagonist effect of peptides **7** and **12** on cell migration (Figure 9). These peptides completely inhibited $VEGF_{165}$-induced cell migration at 100 μM. Moreover, the peptide **7** inhibited, in a dose-dependent manner, $VEGF_{165}$-induced cell migration, with a non-negligible effect at 25 μM and a maximum effect at 50 μM.

Inhibition of $VEGF_{165}$-Induced Capillary Tube Formation on Matrigel. As the peptide **7** inhibited cell migration mediated by VEGF in a dose-dependent manner, it should also be able to block the $VEGF_{165}$-induced endothelial cell differentiation. This phenomenon was analyzed through the capillary tube formation assay on Matrigel, a substrate mimicking basal membrane. Once HUVEC were seeded on Matrigel, $VEGF_{165}$ stimulation (518 pM) induced a capillary tube network composed of cells that migrated and extended to join themselves (Figure 10). Comparatively, the negative control without $VEGF_{165}$ only showed unstructured capillary tube drafts due to the establishment of junctions between cell clusters. In the negative control, capillary tube walls were constituted by many cells, while in the presence of $VEGF_{165}$, they were formed by a very few extended and differentiated cells. The treatment of HUVEC by peptide **7** clearly inhibited the endothelial cells tubulogenesis. Indeed, the number of branching junctions formed by HUVEC on Matrigel was decreased by the action of peptide **7** in a dose-dependent manner, with unstructured capillary tubes formation similar to the negative control when **7** was used at 100 μM and an almost complete capillary tube network at 12.5 μM.

Conclusion

Up to now, most chemical approaches aimed to disturb VEGF−VEGF receptor interactions rely on the identification of peptides isolated by screening of random libraries or phage display method. As a result, little structural information is available which renders the optimization process difficult. Herein, we have exploited the available structural and mutagenesis data to rationally design peptides exhibiting antiangiogenic properties. These peptides were built to mimic, simultaneously, the two VEGF regions constituted by the α-helix 16−27 and the loop 61−68, which remained until now unexploited. As a result of this rational design, we obtained a series of cyclopeptides; the best ones were active at 20−40 μM on VEGF-R1. These results can be positively compared to the low affinity displayed by the peptides targeting only one of these regions.

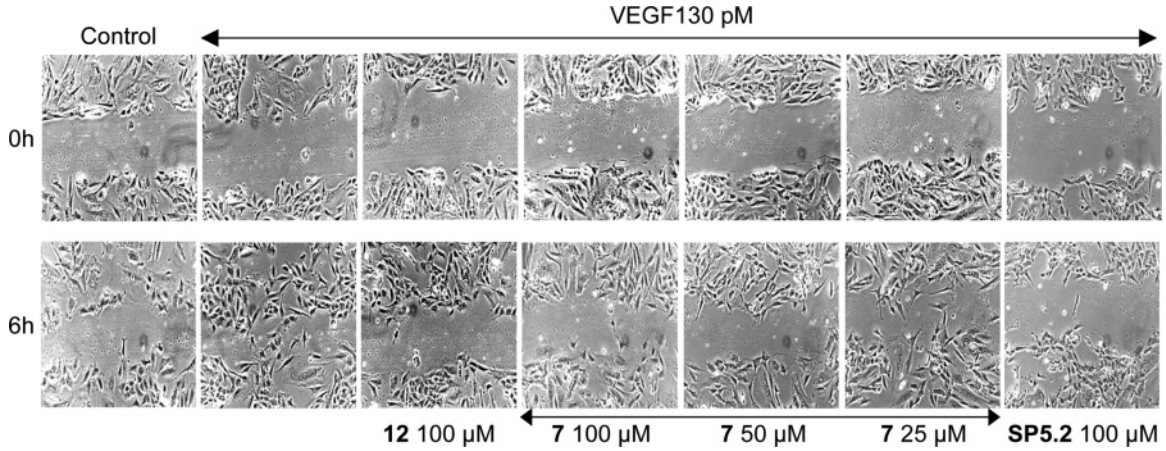

Figure 9. Effect of the peptides on VEGF-induced cell migration in a wound healing assay. Confluent monolayers of starved HUVEC were wounded using a tip, and a set of photos was taken at this time. Then HUVEC were treated with 130 pM of VEGF alone or with the peptides at the indicated concentrations and a second set of photos was taken 6 h later. In the control, HUVEC were incubated with medium 2% FBS. The photos shown are representative of three independent experiments.

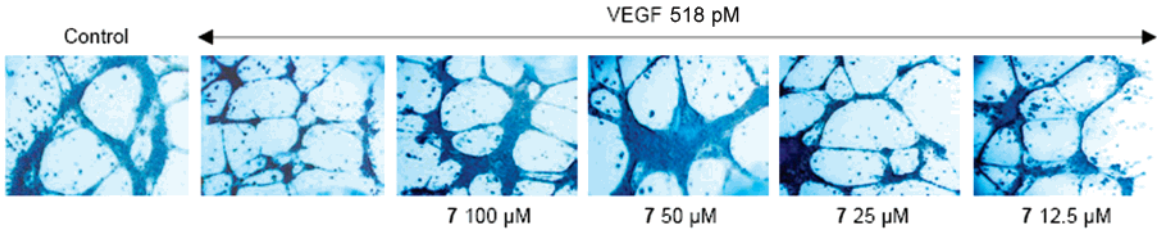

Figure 10. Representative microphotographs of HUVEC on Matrigel showing the effects of peptide **7** on capillary tube formation. HUVEC were treated with 518 pM of VEGF alone or with peptide **7** at the indicated concentrations. Photos were taken after 14 h with a camera at 40× original magnification. The photos shown are representative of three independent experiments.

Moreover, the synthesis of a cyclic peptide incorporating the fluorescent 7-(hydroxycoumar-4-yl)alanine allowed us to verify that these peptides were specific to the VEGF receptors present at the surface of endothelial cells.

The resolution of the structure of the cyclic peptides **4** and **7** by nuclear magnetic resonance (NMR) and molecular modeling using NMR restraints has permitted the obtainment of various information explaining the inhibitory activity of peptide **7**. Following the determination of their 3D structure, their conformation has been compared with the one of the VEGF fragment used as a model to design the cyclic peptide inhibitors. The comparison of their isolated structure and superimposed with the VEGF(61−68) fragment, in interaction with the VEGF-R1 receptor, may possibly explain the difference in the biological activity of each peptide. The docking of peptide **7**, which exhibited the higher inhibitory activity with VEGF-R1 and the minimization of the complex, let us propose that the inhibitory activity of peptide **7** is facilitated by its flexibility by interactions taking place within the complex and stabilized by hydrogen bonds between peptide **7** and VEGF-R1. Finally, the peptide **7** exhibited antagonist activity on endothelial cells. Notably, it was able to inhibit several events implied in angiogenesis processes such as signal transduction, migration, and differentiation on Matrigel. The evaluation of the antitumoral and antiangiogenic activities of these peptides, in vivo, is in progress.

All together, these results illustrate how specific inhibitors can be rationally designed through the structure/function study of the complex and how the inhibitor could be optimized by inspection of its interaction with VEGF-R1. These data could help to propose new molecules targeting the complex formed between VEGF and VEGF-R1.

Materials and Methods

General. Rink amide MBHA resin and HMP resin were purchased from Novabiochem. HBTU, HOBt, DMAP, DCC, and DIPEA were from Applied Biosystems. $Pd(PPh_3)_4$ was from Fluka. All amino acids, from Novabiochem or Bachem, were N^{α}-terminal-protected by Fmoc and their side chains were protected as follows: Arg(*N*-Pmc), Asn(*N*-Trt), Asp(*O*-All), Asp(*O*-*t*-Bu), Cys(*S*-Trt), Cys(*S*-Acm), Gln(*N*-Trt), Glu(*O*-All), Glu(*O*-*t*-Bu), His(*N*-Trt), Lys(*N*-Boc), Ser(*O*-tBu), Thr(*O*-tBu), Trp(*N*-Boc), and Tyr(*O*-*t*Bu). Fmoc-Hca-OH was kindly provided by Dr. Emmanuelle Braud (University Paris Descartes, France). Peptide synthesis solvents and acetonitrile for HPLC were analytical grade and were acquired from commercial sources and used without further purification.

General Procedure for Peptide Synthesis. All peptides were synthesized by Merrifield stepwise solid-phase synthesis on an Applied Biosystems 433A automated peptide synthesizer using standard scale (0.25 mmol) *FastMoc* chemistry. Coupling reactions were performed using Fmoc amino acids (4 equiv), activated with HBTU (4 equiv), and HOBt (4 equiv) in the presence of DIPEA (8 equiv) for 1 h. Fmoc removal was effected by treating the resin with 20% piperidine in NMP for 15 min. Peptides were cleaved from resin with simultaneous removal of side chain protecting groups by treatment with 15 mL of TFA/water/TIPS (95:2.5:2.5 v/v; Method A), TFA/thioanisole/water (94:5:1 v/v; Method B), or TFA/water/EDT/TIPS (94:2.5:2.5:1 v/v; Method C) for 3 h at room temperature. The filtrate from the cleavage reaction was evaporated, precipitated in cold diethyl oxide, collected by centrifugation, and lyophilized.

Peptides Purification and Analysis. Crude peptides were purified by semipreparative RP-HPLC on a Nucleosil C18 column (Vydac, 5 μm, 10 × 250 mm) with a gradient program (solvent A is water with 0.1% TFA and solvent B is 70% acetonitrile aqueous solution with 0.09% TFA) at a flow rate of 2 mL/min with UV detection at 214 and 254 nm. Fractions were analyzed by RP-HPLC on a Nucleosil C18 column (Vydac, 5 μm, 4.6 × 250 mm) at a

flow rate of 1 mL/min and the pure fractions were collected and lyophilized to yield the final peptides as highly purified (>95%) white or off-white solids. The identity of peptides was checked by electrospray mass spectrometry (MS) or by high-resolution electrospray mass spectrometry (HRMS).

Peptide SNDEGLES (1). Synthesis was performed following the general procedure on a HMP resin (substitution: 1.14 mmol/g, 218 mg). Cleavage and deprotection from the resin was realized with method A. Yield after purification, 6.4%; MS *m*/*z* calcd for $C_{32}H_{51}N_9O_{18}$, 849.3; found, 850.7 $[M + H]^+$; $t_R = 8.2$ min (10−30% of solvent B in 20 min, purity 99%).

Peptide Ac-c[CNDEGLEC]-NH$_2$ (2). Synthesis was performed on a Rink amide MBHA resin (substitution: 0.61 mmol/g, 410 mg) with cysteines introduced as Fmoc-Cys(Acm)-OH protected amino acids. The peptide was synthesized following the general procedure, and the N^{α}-terminal amino function was capped by a 20 min treatment with 10 mL of an acetic anhydride mixture (0.5 M acetic anhydride, 0.125 M DIPEA, and 0.015 M HOBt in NMP). Then the resin was suspended in 150 mL of DMF and 50 mL of a solution of iodine in DMF (10 equiv, 632 mg) were added dropwise over 30 min. The solution was stirred vigorously over a period of 5 h at room temperature. The solution was filtered and the resin was washed with 100 mL of DMF and DCM. Deprotection and cleavage of the resin were realized according to method B. Yield after purification, 3.6%; MS *m*/*z* calcd for $C_{34}H_{52}N_{10}O_{16}S_2$, 920.3; found, 921.7 $[M + H]^+$; $t_R = 5.2$ min (20−80% of solvent B in 30 min, purity 97%).

Peptide KFMDVYQRSYCH-NH$_2$ (3). Synthesis was performed on a Rink amide MBHA resin (substitution: 0.61 mmol/g, 410 mg) following the general procedure. Deprotection and cleavage of the resin were realized according to method C. Yield after purification, 3.0%; MS *m*/*z* calcd for $C_{70}H_{102}N_{20}O_{18}S_2$, 1574.7; found, 1576.3 $[M + H]^+$; $t_R = 10.5$ min (20−60% of solvent B in 20 min, purity 98%).

Peptide NGYEIEWYSWVTHGMY-NH$_2$ (SP5.2). Synthesis was performed on a Rink amide MBHA resin (substitution: 0.61 mmol/g, 410 mg) following the general procedure. Deprotection and cleavage of the resin were realized according to method C. Yield after purification, 1.0%; MS *m*/*z* calcd for $C_{96}H_{124}N_{22}O_{26}S$, 2032.9; found, 2034.1 $[M + H]^+$; $t_R = 20.2$ min (20−80% of solvent B in 30 min, purity 91.3%).

General Procedure for Synthesis of Cyclic Peptides 4−12. The linear sequence of amino acids was assembled on Rink amide MBHA resin (substitution: 0.70 mmol/g, 350 mg) according to the general method for peptide synthesis, except that the C-terminal residue was a Fmoc-Glu(*O*-allyl)-OH and the terminal N^{α}-Fmoc protecting group was conserved at the end of the synthesis. After assembling the peptide, the *O*-allyl protecting group on the glutamic acid was removed by the following protocol: the resin was swollen in 30 mL of DCM/AcOH/NMP (37:2:1 v/v) and the suspension was bubbled with argon for 30 min. Then 870 mg of $Pd(PPh_3)_4$ (3 equiv) were added and the solution was stirred for 3 h at room temperature under an argon atmosphere. The suspension was filtered and the resin was washed with a solution of 0.5% DIPEA in NMP (50 mL), a solution of diethyldithiocarbamate (0.5 g in 100 mL NMP), DMF (2 × 10 mL), and DCM (2 × 10 mL). The Fmoc group was then removed with 20% piperidine in NMP (30 min at room temperature) and the resin was washed with NMP. Next the peptidyl resins were stirred overnight with a solution of coupling reagents (8 mL NMP + 0.25 mL 2 M DIPEA in NMP + 2.5 mL 100 mM HBTU in NMP) at room temperature. The resin was washed with NMP and DCM, and the deprotection and cleavage was performed with method A.

Peptide c[hFhFDEGLEE]-NH$_2$ (4). Yield, 17.0%; HRMS *m*/*z* calcd for $C_{47}H_{63}N_9O_{15}Na$, 1016.4311; found, 1016.4339 $[M + Na]^+$; $t_R = 22.1$ min (10−90% of solvent B in 30 min, purity 97.6%).

Peptide c[hFhFDEGLE]-NH$_2$ (5). Yield, 6.9%; HRMS *m*/*z* calcd for $C_{42}H_{56}N_8O_{12}Na$, 887.3915; found, 887.3927 $[M + Na]^+$; $t_R = 24.5$ min (10−90% of solvent B in 30 min, purity 93%).

Peptide c[FFDEGLEE]-NH$_2$ (6). Yield, 9.2%; HRMS *m*/*z* calcd for $C_{45}H_{59}N_9O_{15}Na$, 988.4028; found, 988.4036 $[M + Na]^+$; $t_R = 19.4$ min (10−90% of solvent B in 30 min, purity 94%).

Peptide c[YYDEGLEE]-NH$_2$ (7). Yield, 13.2%; HRMS *m*/*z* calcd for $C_{45}H_{59}N_9O_{17}Na$, 1020.3927; found, 1020.3915 $[M + Na]^+$; $t_R = 14.0$ min (10−90% of solvent B in 30 min, purity 98%).

Peptide c[YWDEGLEE]-NH$_2$ (8). Yield, 8.2%; MS *m*/*z* calcd for $C_{47}H_{60}N_{10}O_{16}$, 1020.4; found, 1021.6 $[M + H]^+$; $t_R = 17.04$ min (10−90% of solvent B in 30 min, purity 90%).

Peptide c[EYDEGLEE]-NH$_2$ (9). Yield, 16.8%; MS *m*/*z* calcd for $C_{41}H_{57}N_9O_{18}$, 963.4; found, 986.5 $[M + Na]^+$; $t_R = 12.47$ min (10−90% of solvent B in 30 min, purity 97%).

Peptide c[YYDEGYEE]-NH$_2$ (10). Yield, 7.5%; MS *m*/*z* calcd for $C_{48}H_{57}N_9O_{18}$, 1047.4; found, 1070.3 $[M + Na]^+$; $t_R = 7.9$ min (20−80% of solvent B in 30 min, purity 99%).

Peptide c[YHcaDEGLEE]-NH$_2$ (11). Yield, 1.0%; MS *m*/*z* calcd for $C_{49}H_{60}N_8O_{17}$, 1065.0; found, 1088.5 $[M + Na]^+$; $t_R = 13.4$ min (20−50% of solvent B in 30 min, purity 98%).

Peptide c[hFHcaDEGLEE]-NH$_2$ (12). Yield, 1.0%; MS *m*/*z* calcd for $C_{49}H_{61}N_9O_{18}$, 1064.1; found, 1064.2 $[M + H]^+$; $t_R = 18.06$ min (10−90% of solvent B in 30 min, purity 95%).

Chemiluminescent Competition Assay on VEGF-R1. The assay was performed as previously described by Goncalves et al.[38] Briefly, a fixed amount of biotinylated $VEGF_{165}$ (131 pM) was incubated with the tested peptide in the presence of recombinant human VEGF-R1 adsorbed on a 96-well microplate. The biotinylated $VEGF_{165}$ remaining after wash steps was detected by chemiluminescence thanks to HRP-conjugated streptavidin.

NMR Experiments and Data Processing. Samples for NMR experiments were prepared by dissolving 1 mg of the cyclic peptide in the solvent mixture H_2O/D_2O/DMSO-d_6 (80:10:10). The pH of the sample was set to 4.1 and 4.24 for the peptides **4** and **7**, respectively. NMR experiments were carried out on an Avance Bruker 600 MHz proton spectrometer. Total COSY, TOCSY,[45] with a mixing time of 70 ms, double quantum filtered spectroscopy, DQF-COSY[46,47] and NOESY[48,49] at five different mixing times (50, 100, 150, 200, and 250 ms) were performed on the samples. Two-dimensional spectra were acquired at 293 K, with 2048 real points in t2, a spectral width of 6010 Hz and 512 t1 increments. The transmitter frequency was set to the water signal. The solvent resonance was suppressed using a 3-9-19 pulse sequence[50] or by saturation of the water signal during the relaxation delay of 1.6 s between free induction decays. For all experiments, the temperature was controlled externally using a temperature control system (BCU 05 Bruker). All data were processed using XWINNMR software (Bruker). A $\pi/6$ phase-shifted sine bell window function was applied and data were zero filled once prior to Fourier transformation in both dimensions t1 and t2. The final size of the frequency domain matrices was 2048 points in ω_1 and ω_2 dimensions. For all experiments, ^{1}H frequency scale was directly referenced to water. The data were then analyzed with the Felix program (Accelrys, San Diego, CA).

Structure Calculation of the Cyclic Peptides. The input distance restraints were deduced from the measurement of the NOE intensities in the NOESY data sets at five mixing times, at the temperature of 293 K, by integration of the peaks into distances by a R-6 dependency and a tolerance of 20% to take into account the errors of integration. The distances were calibrated using the distance between the $\beta1/\beta2$ protons of glutamate residues of 1.76 Å measured in peptide **7** and $\beta1/\beta2$ protons of the aspartic residue for the peptide **4**. No dihedral torsion angle restraints or hydrogen bonds were introduced during the calculations. The structure determination was done using standard protocols of distance geometry and simulated annealing to embed and optimize initial structures and performed with X-PLOR 3.84[41,42] on an SGI O2 R12000 workstation. These structures were optimized further with restrained molecular dynamics simulations, which were carried out in vacuo with a distance-dependent dielectric constant. The dynamics were initiated at 5 K and the temperature was increased gradually to 1000 K in 5.0 ps and then equilibrated for 1.0 ps. The force constants for the distance restraints were kept at 2.0 kcal·mol^{-1}·Å^{-2}

during these stages and were subsequently scaled up to a final value of 30 kcal·mol^{-1}·Å^{-2} over 6.0 ps. The system was then allowed to evolve for 20.0 ps at 1000 K and then slow-cooled to 300 K in 14.0 ps and equilibrated for 10.0 ps. The coordinates saved every 0.5 ps in the last 4.0 ps were averaged. The resulting structures were submitted to a conjugate gradient minimization until a final gradient of 0.1 kcal·mol^{-1}·Å^{-2} was reached. Out of 200 calculated structures, the 10 best structures were selected based on the criteria of acceptable covalent geometry, low distance restraint violations, and favorable nonbonded energy. All dynamics were carried out with a time step of 1.0 fs. The quality of the structures was evaluated with PROCHECK[51] and INSIGHT II (Accelrys) software was used to visualize the structures. The quality of the structures was monitored by pairwise root-mean-squared deviation (rmsd) values and listed in Table 2. The final refined structures of the cyclic peptides in solution exhibit no distance violations larger than 0.2 Å (Table 2). Input restraints statistics are listed in Table 1.

Docking of Peptide 7 on VEGF-R1. To discover the factors favoring the binding of peptide **7** on VEGF-R1 and how this binding could perturb the interaction between the VEGF and its receptor, VEGF-R1, peptide **7** has been docked on VEGF-R1. In a first step, peptide **7** has been superimposed with the VEGF(61−68) fragment, then the VEGF(61−68) has been removed, and the complex formed between VEGF-R1 and peptide **7** has been minimized in a second step. The coordinates of VEGF-R1 have not been allowed to move during the minimization and were maintained fixed with the "constraints-fix-statement" in X-PLOR, while the atoms of peptide **7** have been free to move and to adapt to VEGF-R1. The NOE constraints identified previously within peptide **7** have not been employed during energy minimization. The obtained structure of the complex and the position of peptide **7** on VEGF-R1 have been analyzed, and the hydrogen bond network has been identified between peptide **7** and VEGF-R1.

Cell Line and Culture. HUVEC were obtained as a gift from Dr. Catherine Boisson-Vidal (U765 INSERM) and were cultured in 150 cm^2 plastic flasks, coated by a solution of 0.5% gelatin (BioChemika, Sigma), in M199 containing 20% fetal bovine serum (FBS). Cells were incubated at 37 °C in a humidified atmosphere of 5% CO_2 in air, and medium was changed every two days. Experiments were conducted on HUVEC that had gone through one to five passages.

Imaging of the Binding between the Peptide 12 and the VEGF Receptors. HUVEC were grown on six-well plates coated by a solution of 0.5% gelatine containing a slide. Preconfluent HUVEC were incubated with **12** and $VEGF_{165}$ at indicated concentrations for 6 h. After this time, cells were washed three times with PBS and fixed with 4% formaldehyde. Cells were washed three times with PBS, and slides were mounted using mounting medium Vectashield Hard set (Vector Laboratories, Burlingame). The binding between **12** and HUVEC was analyzed with a biphotonic confocal microscope (Leica TCS SP2 AOBS, laser 2 photons: Tsunami, Spectra Physics; Institut Jacques Monod, France). Experiments were repeated two times with identical results.

Western Blot Analysis. Experiments were realized in six-well plates coated with a solution of 0.5% gelatin. HUVEC, at confluence, were starved in 2% FBS-supplemented M199 overnight, followed by 5 h in 0% FBS-supplemented M199. HUVEC were treated for 20 min by compounds at the indicated concentrations in 0% FBS-supplemented M199 and then stimulated by $VEGF_{165}$ at 130 pM during 10 min. Cells were washed three times with ice-cold PBS, and the reaction was terminated by the addition of 100 μL of ice-cold lysis buffer HNTG : Hepes 50 mM, NaCl 150 mM, glycerol 10%, Triton 100 1%, EGTA 1 mM, $MgCl_2$ 1 mM, Na_3VO_4 1 mM, NaF 1 mM, and one protease inhibitor cocktail tablet (Complete, Roche). Equivalent amounts of proteins from each lysate were resolved in 12% SDS-polyacrylamide gel and then transferred onto nitrocellulose membranes (Bio-Rad Laboratories). The transblotted membrane was incubated with antiphosphorylated p44−42 ERK MAPK antibody (Cell Signaling Technology, Beverly, MA, Etats-Unis; 1:1000) and with anti-γ-tubuline (Santa Cruz Biotechnology, Californie, Etats-Unis; 1:1000) in Tris-HCl buffered saline (TBS) containing 0.1% Tween 20 (TBST) and 5% FBS at 4 °C overnight. After treatment with the primary antibody, the membrane was washed three times with TBST, then incubated with anti-rabbit IgG-horseradish peroxidase conjugates (Amersham Biosciences, Buckinghamshire, Angleterre; 1:6000) for 1 h at room temperature, and washed three times with TBST. The immunoblots were visualized by enhanced chemiluminescence (Amersham Biosciences).

Wound Healing Assay. HUVEC were seeded in six-well plates coated with a solution of 0.5% gelatin and were allowed to grow to confluence. Complete medium was replaced by medium containing 2% FBS, and incubation was continued overnight. A linear wound was drawn in the monolayer of cells. A set of digital photos was taken of each wound with a camera (Digital Sight, DS-L1, Nikon, Japon) at 100× original magnification. The wells were washed with PBS, and medium containing 130 pM $VEGF_{165}$ in the presence or absence of peptides at 100 μM was added. After 6 h, a second set of photos was taken at the same place in the same conditions.

Capillary Tube Formation on Matrigel (In Vitro Angiogenesis Assay). The formation of capillary tube-like structures by HUVEC was analyzed on 96-well plates coated with growth factor reduced MATRIGEL matrix (BD Biosciences, U.S.A.). Matrigel was thawed at 4 °C. Then 75 μL/well of Matrigel was distributed and allowed to solidify at 37 °C over a period of 1 h. HUVEC were seeded on the polymerized Matrigel (2×10^4 cells/well) in medium containing 5% FBS, with 518 pM of VEGF in the presence or absence of **7** at the indicated concentrations. The plate was incubated at 37 °C, and tube formation was observed after 14 h under a phase-contrast microscope. Digital pictures were then taken with a camera (Digital Sight, DS-L1, Nikon, Japon) at 40× original magnification.

Acknowledgment. Financial support for this work was provided by the Ligue nationale contre le cancer and by the University Paris Descartes Bonus-Qualité-Recherche grant. The authors thank Dr. W.-Q. Liu for mass spectral data, Dr. C. Boisson-Vidal and I. Galy-Fauroux for providing HUVE cells, and C. Piolot and C. Chamot for their support for biphotonic microscopy experiments.

Supporting Information Available: ^{1}H NMR spectra of compounds **4** and **7** in DMSO-d_6; table of purity for the target compounds **1**−**12** and **SP5.2**; and HPLC analysis for the target compounds **1**−**12** and **SP5.2**. This material is available free of charge via the Internet at http://pubs.acs.org.

References

(1) Ferrara, N. Vascular endothelial growth factor: Basic science and clinical progress. *Endocr. Rev.* **2004**, *25*, 581−611.
(2) Carmeliet, P.; Jain, R. K. Angiogenesis in cancer and other diseases. *Nature* **2000**, *407*, 249−257.
(3) Ferrara, N.; Kerbel, R. S. Angiogenesis as a therapeutic target. *Nature* **2005**, *438*, 967−974.
(4) Kerbel, R. S. Antiangiogenic therapy: a universal chemosensitization strategy for cancer? *Science* **2006**, *312*, 1171−1175.
(5) Ferrara, N.; Gerber, H. P. The role of vascular endothelial growth factor in angiogenesis. *Acta Haematol.* **2001**, *106*, 148−156.
(6) Olsson, A. K.; Dimberg, A.; Kreuger, J.; Claesson-Welsh, L. VEGF receptor signalling - in control of vascular function. *Nat. Rev. Mol. Cell. Biol.* **2006**, *7*, 359−371.
(7) Roskoski, R., Jr. Vascular endothelial growth factor (VEGF) signaling in tumor progression. *Crit. Rev. Oncol. Hematol.* **2007**, *62*, 179−213.
(8) Takahashi, H.; Shibuya, M. The vascular endothelial growth factor (VEGF)/VEGF receptor system and its role under physiological and pathological conditions. *Clin. Sci. (London)* **2005**, *109*, 227−241.
(9) Luttun, A.; Autiero, M.; Tjwa, M.; Carmeliet, P. Genetic dissection of tumor angiogenesis: Are PlGF and VEGFR-1 novel anticancer targets? *Biochim. Biophys. Acta* **2004**, *1654*, 79−94.
(10) Karashima, T.; Inoue, K.; Fukata, S.; Iiyama, T.; Kurabayashi, A.; Kawada, C.; Shuin, T. Blockade of the vascular endothelial growth factor-receptor 2 pathway inhibits the growth of human renal cell carcinoma, RBM1-IT4, in the kidney but not in the bone of nude mice. *Int. J. Oncol.* **2007**, *30*, 937−45.

(11) Gille, J.; Heidenreich, R.; Pinter, A.; Schmitz, J.; Boehme, B.; Hicklin, D. J.; Henschler, R.; Breier, G. Simultaneous blockade of VEGFR-1 and VEGFR-2 activation is necessary to efficiently inhibit experimental melanoma growth and metastasis formation. *Int. J. Cancer*. **2007**, *120*, 1899−1908.
(12) Laakkonen, P.; Waltari, M.; Holopainen, T.; Takahashi, T.; Pytowski, B.; Steiner, P.; Hicklin, D.; Persaud, K.; Tonra, J. R.; Witte, L.; Alitalo, K. Vascular endothelial growth factor receptor 3 is involved in tumor angiogenesis and growth. *Cancer Res.* **2007**, *67*, 593−599.
(13) Soker, S.; Miao, H. Q.; Nomi, M.; Takashima, S.; Klagsbrun, M. VEGF165 mediates formation of complexes containing VEGFR-2 and neuropilin-1 that enhance VEGF165-receptor binding. *J. Cell. Biochem.* **2002**, *85*, 357−368.
(14) Sandler, A.; Gray, R.; Perry, M. C.; Brahmer, J.; Schiller, J. H.; Dowlati, A.; Lilenbaum, R.; Johnson, D. H. Paclitaxel-carboplatin alone or with bevacizumab for non-small-cell lung cancer. *N. Engl. J. Med.* **2006**, *355*, 2542−2550.
(15) Sun, S.; Schiller, J. H. Angiogenesis inhibitors in the treatment of lung cancer. *Crit. Rev. Oncol. Hematol.* **2007**, *62*, 93−104.
(16) Holash, J.; Davis, S.; Papadopoulos, N.; Croll, S. D.; Ho, L.; Russell, M.; Boland, P.; Leidich, R.; Hylton, D.; Burova, E.; Ioffe, E.; Huang, T.; Radziejewski, C.; Bailey, K.; Fandl, J. P.; Daly, T.; Wiegand, S. J.; Yancopoulos, G. D.; Rudge, J. S. VEGF-Trap: A VEGF blocker with potent antitumor effects. *Proc. Natl. Acad. Sci. U.S.A.* **2002**, *99*, 11393−11398.
(17) Parry, T. J.; Cushman, C.; Gallegos, A. M.; Agrawal, A. B.; Richardson, M.; Andrews, L. E.; Maloney, L.; Mokler, V. R.; Wincott, F. E.; Pavco, P. A. Bioactivity of antiangiogenic ribozymes targeting Flt-1 and KDR mRNA. *Nucleic Acids Res.* **1999**, *27*, 2569−2577.
(18) Gragoudas, E. S.; Adamis, A. P.; Cunningham, E. T., Jr.; Feinsod, M.; Guyer, D. R. Pegaptanib for neovascular age-related macular degeneration. *N. Engl. J. Med.* **2004**, *351*, 2805−2816.
(19) Goncalves, V. G. B.; Lenoir, C.; Garbay, C.; Vidal, M.; Inguimbert, N. Peptides as antagonists of the VEGF receptors. *Pharmachem* **2006**, 15−19.
(20) D'Andrea, L. D.; Del Gatto, A.; Pedone, C.; Benedetti, E. Peptide-based molecules in angiogenesis. *Chem. Biol. Drug. Des.* **2006**, *67*, 115−126.
(21) Jia, H.; Jezequel, S.; Lohr, M.; Shaikh, S.; Davis, D.; Soker, S.; Selwood, D.; Zachary, I. Peptides encoded by exon 6 of VEGF inhibit endothelial cell biological responses and angiogenesis induced by VEGF. *Biochem. Biophys. Res. Commun.* **2001**, *283*, 164−173.
(22) Wiesmann, C.; Fuh, G.; Christinger, H. W.; Eigenbrot, C.; Wells, J. A.; de Vos, A. M. Crystal structure at 1.7 A resolution of VEGF in complex with domain 2 of the Flt-1 receptor. *Cell* **1997**, *91*, 695−704.
(23) Davis-Smyth, T.; Chen, H.; Park, J.; Presta, L. G.; Ferrara, N. The second immunoglobulin-like domain of the VEGF tyrosine kinase receptor Flt-1 determines ligand binding and may initiate a signal transduction cascade. *Emb. J.* **1996**, *15*, 4919−4927.
(24) Barleon, B.; Totzke, F.; Herzog, C.; Blanke, S.; Kremmer, E.; Siemeister, G.; Marme, D.; Martiny-Baron, G. Mapping of the sites for ligand binding and receptor dimerization at the extracellular domain of the vascular endothelial growth factor receptor FLT-1. *J. Biol. Chem.* **1997**, *272*, 10382−10388.
(25) Cunningham, S. A.; Stephan, C. C.; Arrate, M. P.; Ayer, K. G.; Brock, T. A. Identification of the extracellular domains of Flt-1 that mediate ligand interactions. *Biochem. Biophys. Res. Commun.* **1997**, *231*, 596−599.
(26) Fuh, G.; Li, B.; Crowley, C.; Cunningham, B.; Wells, J. A. Requirements for binding and signaling of the kinase domain receptor for vascular endothelial growth factor. *J. Biol. Chem.* **1998**, *273*, 11197−11204.
(27) Herley, M. T.; Yu, Y.; Whitney, R. G.; Sato, J. D. Characterization of the VEGF binding site on the Flt-1 receptor. *Biochem. Biophys. Res. Commun.* **1999**, *262*, 731−738.
(28) Muller, Y. A.; Li, B.; Christinger, H. W.; Wells, J. A.; Cunningham, B. C.; de Vos, A. M. Vascular endothelial growth factor: Crystal structure and functional mapping of the kinase domain receptor binding site. *Proc. Natl. Acad. Sci. U.S.A.* **1997**, *94*, 7192−7197.
(29) Christinger, H. W.; Fuh, G.; de Vos, A. M.; Wiesmann, C. The crystal structure of placental growth factor in complex with domain 2 of vascular endothelial growth factor receptor-1. *J. Biol. Chem.* **2004**, *279*, 10382−10388.
(30) Keyt, B. A.; Nguyen, H. V.; Berleau, L. T.; Duarte, C. M.; Park, J.; Chen, H.; Ferrara, N. Identification of vascular endothelial growth factor determinants for binding KDR and FLT-1 receptors. Generation of receptor-selective VEGF variants by site-directed mutagenesis. *J. Biol. Chem.* **1996**, *271*, 5638−5646.
(31) Zilberberg, L.; Shinkaruk, S.; Lequin, O.; Rousseau, B.; Hagedorn, M.; Costa, F.; Caronzolo, D.; Balke, M.; Canron, X.; Convert, O.; Lain, G.; Gionnet, K.; Goncalves, M.; Bayle, M.; Bello, L.; Chassaing, G.; Deleris, G.; Bikfalvi, A. Structure and inhibitory effects on angiogenesis and tumor development of a new vascular endothelial growth inhibitor. *J. Biol. Chem.* **2003**, *278*, 35564−35573.
(32) Berthelot, T.; Goncalves, M.; Lain, G.; Estieu-Gionnet, K.; Deleris, G. New strategy towards the efficient solid phase synthesis of cyclopeptides. *Tetrahedron* **2006**, *62*, 1124−1130.
(33) D'Andrea, L. D.; Iaccarino, G.; Fattorusso, R.; Sorriento, D.; Carannante, C.; Capasso, D.; Trimarco, B.; Pedone, C. Targeting angiogenesis: Structural characterization and biological properties of a de novo engineered VEGF mimicking peptide. *Proc. Natl. Acad. Sci. U.S.A.* **2005**, *102*, 14215−14220.
(34) Chang, C. D.; Meienhofer, J. Solid-phase peptide-synthesis using mild base cleavage of nalpha-fluorenylmethyloxycarbonylamino acids, exemplified by a synthesis of dihydrosomatostatin. *Int. J. Pept. Protein Res.* **1978**, *11*, 246−249.
(35) Joseph, C. G.; Wang, X. S.; Scott, J. W.; Bauzo, R. M.; Xiang, Z.; Richards, N. G.; Haskell-Luevano, C. Stereochemical studies of the monocyclic agouti-related protein (103−122) Arg-Phe-Phe residues: Conversion of a melanocortin-4 receptor antagonist into an agonist and results in the discovery of a potent and selective melanocortin-1 agonist. *J. Med. Chem.* **2004**, *47*, 6702−6710.
(36) Mazur, S.; Jayalekshmy, P. Chemistry of polymer-bound *ortho*-benzyne−Frequency of encounter between substituents on cross-linked polystyrenes. *J. Am. Chem. Soc.* **1979**, *101*, 677−683.
(37) El-Mousawi, M.; Tchistiakova, L.; Yurchenko, L.; Pietrzynski, G.; Moreno, M.; Stanimirovic, D.; Ahmad, D.; Alakhov, V. A vascular endothelial growth factor high affinity receptor 1-specific peptide with antiangiogenic activity identified using a phage display peptide library. *J. Biol. Chem.* **2003**, *278*, 46681−46691.
(38) Goncalves, V.; Gautier, B.; Garbay, C.; Vidal, M.; Inguimbert, N. Development of a chemiluminescent screening assay for detection of vascular endothelial growth factor receptor 1 ligands. *Anal. Biochem.* **2007**, *366*, 108−110.
(39) Alcaro, M. C.; Sabatino, G.; Uziel, J.; Chelli, M.; Ginanneschi, M.; Rovero, P.; Papini, A. M. On-resin head-to-tail cyclization of cyclotetrapeptides: Optimization of crucial parameters. *J. Pept. Sci.* **2004**, *10*, 218−228.
(40) Nilges, M.; Clore, G. M.; Gronenborn, A. M. Determination of 3-dimensional structures of proteins from interproton distance data by hybrid distance geometry-dynamical simulated annealing calculations. *FEBS Lett.* **1988**, *229*, 317−324.
(41) Laskowski, R. A.; Rullmann, J. A. C.; MacArthur, M. W.; Kaptein, R.; Thornton, J. M. AQUA and PROCHECK-NMR: Programs for checking the quality of protein structures solved by NMR. *J. Biomol. NMR* **1996**, *8*, 477−486.
(42) Brünger, A. T. *X-PLOR Software Manual*, version 3.1; Yale University Press: New Haven, CT, 1992.
(43) Brun, M. P.; Bischoff, L.; Garbay, C. A very short route to enantiomerically pure coumarin-bearing fluorescent amino acids. *Angew. Chem., Int. Ed.* **2004**, *43*, 3432−3436.
(44) Cross, M. J.; Claesson-Welsh, L. FGF and VEGF function in angiogenesis: Signalling pathways, biological responses and therapeutic inhibition. *Trends Pharmacol. Sci.* **2001**, *22*, 201−207.
(45) Griesinger, C.; Otting, G.; Wuthrich, K.; Ernst, R. R. Clean TOCSY for H-1 spin system-identification in macromolecules. *J. Am. Chem. Soc.* **1988**, *110*, 7870−7872.
(46) Rance, M.; Sorensen, O. W.; Bodenhausen, G.; Wagner, G.; Ernst, R. R.; Wuthrich, K. Improved spectral resolution in COSY H-1-NMR spectra of proteins via double quantum filtering. *Biochem. Biophys. Res. Commun.* **1983**, *117*, 479−485.
(47) Marion, D.; Wuthrich, K. Application of phase sensitive two-dimensional correlated spectroscopy (COSY) for measurements of H-1−H-1 spin−spin coupling-constants in proteins. *Biochem. Biophys. Res. Commun.* **1983**, *113*, 967−974.
(48) Jeener, J.; Meier, B. H.; Bachmann, P.; Ernst, R. R. Investigation of exchange processes by 2-dimensional NMR spectroscopy. *J. Chem. Phys.* **1979**, *71*, 4546−4553.
(49) Kumar, A.; Ernst, R. R.; Wuthrich, K. A two-dimensional nuclear Overhauser enhancement (2D NOE) experiment for the elucidation of complete proton−proton cross-relaxation networks in biological macromolecules. *Biochem. Biophys. Res. Commun.* **1980**, *95*, 1−6.
(50) Piotto, M.; Saudek, V.; Sklenar, V. Gradient-tailored excitation for single-quantum NMR-spectroscopy of aqueous solutions. *J. Biomol. NMR* **1992**, *2*, 661−665.
(51) Wüthrich, K. *NMR of Proteins and Nucleic Acids*; Wiley-Interscience: New York, 1986.

JM0706970